Laboratory Measurements of Coseismic Fields: Toward a Validation of Pride's Theory

Clarisse Bordes, Daniel Brito, Julia Holzhauer, Laurence Jouniaux, Stéphane Garambois, Michel Dietrich

Laboratory measurements of coseismic fields: towards a validation of Pride's theory

C. Bordes[1], D. Brito[1], J. Holzhauer[1], L. Jouniaux[2], S. Garambois[3], M. Dietrich[3]

[1]LFCR, UMR 5150, Total-CNRS-Université de Pau et des Pays de l'Adour, France

[2]IPGS, UMR 7516, CNRS-Université de Strasbourg, France

[3]ISTerre, UMR 5275, CNRS-IRD-Université Grenoble Alpes, France

1 Introduction

As discussed in previous chapters, seismoelectric phenomenon was first theoretically described in 1944 [*Frenkel*, 2005]. More recently, in his reference paper, *Pride* [1994] developed the whole set of governing equations in a saturated medium. These equations couple the Biot theory for seismic propagation in porous medium [*Biot*, 1956a,b] and Maxwell's equations for electromagnetism, via fluid and charge transport equations using a volume averaging approach. Pride's full seismoelectric analytical formulation has been largely used in recent years for numerical computations [*Garambois and Dietrich*, 2002; *Guan and Hu*, 2008; *Zyserman et al.*, 2010; *Santos et al.*, 2012; *Zyserman et al.*, 2012; *Warden et al.*, 2013; *Zyserman et al.*, 2015] in order to discuss potential applications of seismoelectrics as a geophysical probing method. In the last decade, seismoelectric phenomena were also discussed by considering electrokinetic couplings as a function of the charge density [*Revil and Jardani*, 2010; *Revil and Mahardika*, 2013; *Jougnot et al.*, 2013; *Revil et al.*, 2013].

The two main effects generated by electrokinetic coupling are i) coseismic field accompanying the seismic propagation and ii) electromagnetic disturbances generated at depth when seismic waves are crossing an interface. The seismoelectric interface conversion is often perceived as a promising tool for reservoir characterization since it is expected to combine both electrical and mechanical sensitivities [*Garambois and Dietrich*, 2002; *Haines et al.*, 2007; *Dupuis et al.*, 2007]. The coseismic part is therefore considered as a strong disturbance to be removed for enhancing the interface response [*Warden et al.*, 2012]. However, coseismic phenomenon may also be perceived as a direct observation of fluid motions occurring with seismic propagation. Indeed, these relative fluid displacements are involved in attenuation and dispersion of seismic waves as discussed in

the original Biot theory and in many more recent poroelastic studies [*Pride and Berryman*, 2003a,b; *Müller and Gurevich*, 2004; *Müller et al.*, 2010]. The quantitative interpretation of this coseismic contribution would be therefore a powerful and original approach for testing many of these poroelastic issues. In this paper, we aim to show this quantitative interpretation to be within reach, the first step being the validation of Pride's theory.

When seismic waves are travelling in a porous medium, the coseismic seismoelectric field $\mathbf{E}$ is expected to be coupled to all propagation modes. As predicted by *Biot* [1956a,b] body waves are travelling as fast P_f, slow P_s and S waves. The $\mathbf{E}$ field can therefore be written as a function of seismic displacements by using the Helmholtz decomposition [*Hu et al.*, 2000]:

$$\mathbf{E} = \beta_{P_f} A_{P_f} \nabla\Phi_{P_f} + \beta_{P_s} A_{P_s} \nabla\Phi_{P_s} + \beta_S A_S \nabla \times \Gamma_S \tag{1}$$

where A_i and β_i ($i = P_f, P_s$ or S) are the amplitudes and seismoelectric couplings of each mode. Φ_{P_i} are the potential functions of P waves (that are pure divergence) and Γ_S is the potential vector of S waves (that is pure curl). Hence, the contributions of P waves are vanishing in seismomagnetic field that is obtained by the fundamental Maxwell equation:

$$\mathbf{H} = -\frac{i}{\omega\mu}\nabla \times \mathbf{E} = -\frac{i}{\omega\mu}\beta_S A_S \nabla \times \nabla \times \Gamma_S \tag{2}$$

where ω is the pulsation of the seismic wave whose time dependence is supposed to be $e^{-i\omega t}$, and μ is the magnetic permeability of the porous medium ($\mu \simeq \mu_0 = 4\pi 10^{-7}\ V.s.A^{-1}.m^{-1}$ in non-metallic rocks). Indeed, equation (2) shows the seismomagnetic field to be generated by S waves when all body waves are supposed to contribute to the seismoelectric field. Nevertheless, the effectiveness of S waves in seismoelectric field must be discussed relatively to the contribution of P waves, the simplest way to address this issue being the transfer function approach as proposed by *Pride and Haartsen* [1996]. Considering both fast and slow P waves, the seismoelectric field can be written as a function of local accelerations $\ddot{\mathbf{U}}_i$ following [*Garambois and Dietrich*, 2001; *Bordes et al.*, 2015]:

$$\mathbf{E}(\omega) = \psi_{\mathrm{Pf}}(\omega)\ddot{\mathbf{U}}_{\mathrm{Pf}}(\omega) + \psi_{\mathrm{Ps}}(\omega)\ddot{\mathbf{U}}_{\mathrm{Ps}}(\omega) + \psi_{\mathrm{S}}(\omega)\ddot{\mathbf{U}}_{\mathrm{S}}(\omega) \tag{3}$$

where ψ_{Pi} and ψ_{S} are respectively the complex dynamic transfer functions for P (fast or slow) and S waves defined by:

$$\psi_{\mathrm{Pi}}(\omega) = \frac{i}{\omega}\frac{\tilde{\rho}(\omega)L(\omega)}{\tilde{\varepsilon}(\omega)}\frac{Hs^2_{\mathrm{Pi}}(\omega) - \rho}{Cs^2_{\mathrm{Pi}}(\omega) - \rho_f} \tag{4}$$

and

$$\psi_{\mathrm{S}}(\omega) = \frac{i}{\omega}\mu\tilde{\rho}(\omega)L(\omega)\frac{G}{\rho_f}\frac{s_{\mathrm{S}}^2(\omega) - \rho/G}{s_{\mathrm{S}}^2(\omega) - \mu\tilde{\varepsilon}(\omega)}. \tag{5}$$

In equations (4) and (5), $\rho = \phi\rho_f + (1-\phi)\rho_s$ is the total density of the porous medium composed of fluid and solid phases whose respective densities are ρ_f and ρ_s. G is the shear modulus of the frame, $H = K_U + \frac{4}{3}G$ is the P wave modulus, K_U is the undrained bulk modulus (known as "Gassman's modulus" as well), and $C = BK_U$ derives from the Skempton's coefficient B that can be deduced from the porosity ϕ and from fluid and solid bulk moduli K_f and K_s [*Barriere et al.*, 2012]. The slownesses s_{Pi} (P waves) and s_{S} (S waves), including both Biot's and electrokinetic losses, will be given in equations (14). *Pride and Haartsen* [1996] used the following formulations of the effective electrical permittivity:

$$\tilde{\varepsilon}(\omega) = \varepsilon(\omega) + \frac{i}{\omega}\sigma(\omega) - \tilde{\rho}(\omega)L^2(\omega) \tag{6}$$

and of the effective density of the fluid in relative motion

$$\tilde{\rho} = \frac{i}{\omega}\frac{\eta_f}{k(\omega)}, \tag{7}$$

where η_f is the dynamic viscosity of the fluid. In this formulation, the effect of Biot's losses is carried by the dynamic permeability [*Johnson et al.*, 1987]:

$$k(\omega) = k_0\left[\left(1 - i\frac{\omega}{\omega_c}\frac{4}{m_p}\right)^{\frac{1}{2}} - i\frac{\omega}{\omega_c}\right]^{-1}, \tag{8}$$

where k_0 is the intrinsic permeability of the medium and m_p is a pore space term. The Biot pulsation ω_c or frequency f_c defines the limit between low and high frequency domains for which energy dissipation is respectively due to viscous or inertial flows:

$$\omega_c = 2\pi f_c = \frac{\eta_f}{F\rho_f k_0}. \tag{9}$$

where F is the formation factor and ρ_f is the fluid density. The frequency dependent electrokinetic coupling $L(\omega)$ in equations (4), (5) and (6) is defined as:

$$L(\omega) = L_0\left[1 - i\frac{\omega}{\omega_c}\frac{m_p}{4}\left(1 - 2\frac{\tilde{d}}{\Lambda}\right)^2\left(1 - i^{3/2}\frac{\tilde{d}}{\delta}\right)^2\right]^{-\frac{1}{2}} \simeq L_0\left[1 - i\frac{\omega}{\omega_c}\frac{m_p}{4}\right]^{-\frac{1}{2}}. \tag{10}$$

In this equation, $\Lambda = \sqrt{m_P k_0 F}$ is a pore-shape parameter, $\delta = \sqrt{\eta_f/\omega\rho_f}$ is the skin depth and $\tilde{d} = 10^{-6}\delta\sqrt{\omega/2\pi C}$ is the thickness of the double layer [*Pride*, 1994]. We notice that neglecting both terms in parentheses of equation (10) gives a more handy expression of L and represents a very tiny error (less than few percents). Eventually, L_0 is the low

frequency coupling that can be defined as:

$$L_0 = -\frac{C_{ek}\sigma_f}{F}\left(1 - \frac{2\tilde{d}}{\Lambda}\right) \simeq -\frac{C_{ek}\sigma_f}{F}. \tag{11}$$

where F is the formation factor from Archie's law and σ_f is the fluid's conductivity. The C_{ek} coefficient is often called the electrokinetic coefficient. It characterizes the linear relation between the potential gradient ΔV and the pressure gradient ΔP involved in a steady state fluid circulation ($C_{ek} = \Delta V/\Delta P$). This coefficient may be expressed as a function of the volumetric charge density and the hydraulic conductivity [*Bolève et al.*, 2007] but this dependence to hydraulic properties may be debated [*Jouniaux and Zyserman*, 2015]. For laminar flows, it can also be expressed by the Helmholtz-Smoluchowski equation [*Overbeek*, 1952] on the condition that the surface conductivity can be neglected:

$$C_{ek} = \frac{\epsilon_f \zeta}{\eta_f \sigma_f} \tag{12}$$

where ζ is the zeta potential itself depending on pH, mineral and fluid composition [*Jouniaux and Zyserman*, 2016]. By compiling numerous streaming potential studies in sand and sandstones, *Jouniaux and Ishido* [2012] proposed the simple empirical relation $C_{ek} = -1.2 \text{ x } 10^{-8}\sigma_f^{-1}$ directly linking the electrokinetic coefficient to the fluid conductivity in the $\sigma_f = [10^{-3} - 10^{1}]\ S/m$ range.

Eventually, the slownesses of longitudinal P and transverse S waves are given by *Pride and Haartsen* [1996] for plane waves:

$$\begin{aligned}
s_P(\omega) &= \left[\frac{1}{2}\gamma(\omega) - \frac{1}{2}\sqrt{\gamma(\omega)^2 - \frac{4\tilde{\rho}(\omega)\rho}{MH - C^2}\left(\frac{\rho_t}{\rho} + \frac{\tilde{\rho}(\omega)L(\omega)^2}{\tilde{\varepsilon}(\omega)}\right)}\right]^{1/2}, \\
s_S(\omega) &= \left[\frac{1}{2}\frac{\rho_t}{G} + \frac{1}{2}\mu\tilde{\varepsilon}(\omega)\left(1 + \frac{\tilde{\rho}(\omega)L(\omega)^2}{\tilde{\varepsilon}(\omega)}\right)\right. \\
&\quad \left. + \frac{1}{2}\sqrt{\left[\frac{\rho_t}{G} - \mu\tilde{\varepsilon}(\omega)\left(1 + \frac{\tilde{\rho}(\omega)L(\omega)^2}{\tilde{\varepsilon}(\omega)}\right)\right]^2 - 4\mu\frac{\rho_f^2 L(\omega)^2}{G}}\right]^{1/2} \\
\text{with } \gamma(\omega) &= \frac{\rho M + \tilde{\rho}(\omega)H\left(1 + \tilde{\rho}(\omega)L(\omega)^2/\tilde{\varepsilon}(\omega)\right) - 2\rho_f C}{HM - C^2}.
\end{aligned} \tag{13}$$

From this set of equations and the parameters of table (1) we get the magnitudes of the seismoelectric transfer functions of P_i ($i = f$ for fast P and $i = s$ for slow P) and S waves in quartz sand and sandstone (figure 1). In all ψ_{Pi} and ψ_{S} curves, the low and high frequency limits are pretty obvious: each curve tends to a different asymptote appart of the Biot frequency. We particularly notice the low frequency limit of ψ_{Pi} tending to a non-dynamic (linear) transfer function, as expected by *Garambois and Dietrich*

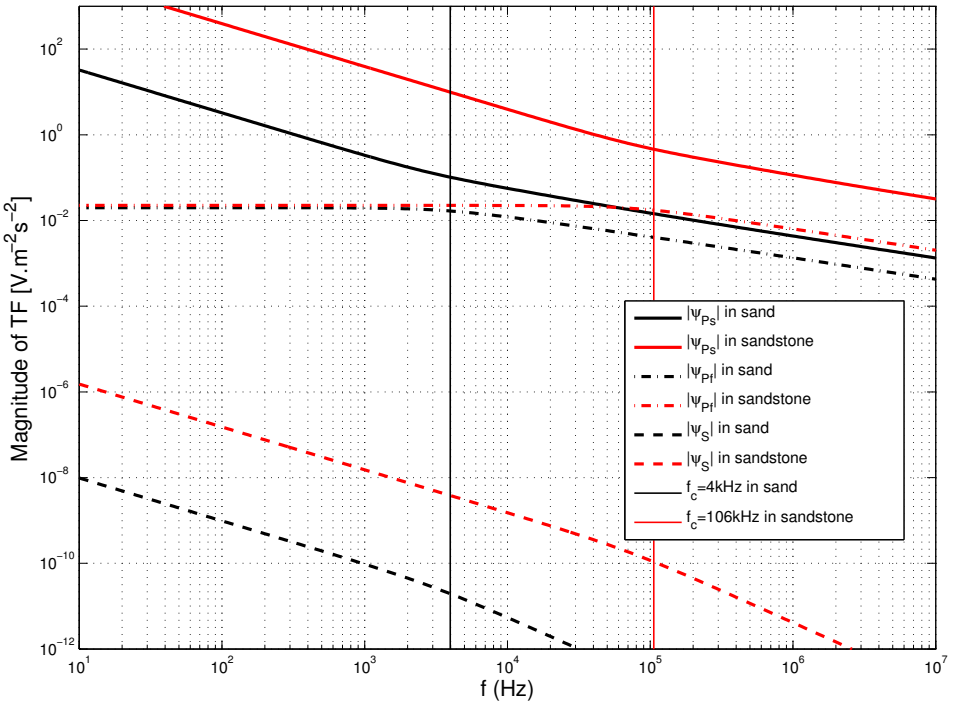

Figure 1. Magnitudes of dynamic transfer functions of slow P (ψ_{Ps}), fast P (ψ_{Pf}) and *S* waves (ψ_{S}) computed for water filled quartz sand (black curves) and sandstone (red curves), and respective Biot's frequencies f_c.

[2001]. The magnitude ψ_{S} is very low compared to that of ψ_{Pi}, and it seems very difficult to observe the seismoelectric field associated to the propagation of shear wave. This is a very interesting point since, as discussed above, the contribution of *P* waves is negligible in seismomagnetic field: it theoretically seems that measuring both seismoelectric and seismomagnetic fields would be an original way for separating *P* and *S* waves in a mixed seismic propagation. We also notice the ψ_{Ps} transfer function to be very large compared to ψ_{Pf}. The Biot slow wave is therefore expected to be enhanced in seismoelectric fields, especially in the diffusive regime [*Garambois and Dietrich*, 2013]. Indeed, measuring the seismoelectric transfer functions would be an original and promising way to experience the Biot slow wave, that is still poorly observed and understood [*Garambois and Dietrich*, 2013].

In the purpose of providing original observations for these fundamental poroelasticity issues, we aim to validate the Pride theory by performing laboratory experiments under controlled conditions. In section 2, we discuss some issues or questions that might be en-

123 **Table 1.** Parameters used for the computation of seismoelectric transfer functions of figure 1 in quartz sand
124 and sandstone.

Parameter	**Notation**	**Unit**	**Value**
			Waterfilled sand / sandstone
Porosity	ϕ		0.4 / 0.15
Formation factor	F		4 / 15
Intrinsic permeability	k_0	$m.s^{-2}$	10^{-11} / 10^{-13}
Bulk modulus of the solid	K_s	GPa	0.02 / 1
Bulk modulus of the fluid	K_f	GPa	0.02 / 1
Bulk modulus of the frame	K_{fr}	GPa	0.02 / 1
Shear modulus of the frame	G	GPa	0.012 / 0.6
Density of the solid (quartz)	ρ_s	$kg.m^{-3}$	2650
Density of the fluid (water)	ρ_f	$kg.m^{-3}$	1000
Electrical conductivity of the fluid	σ_f	$S.m^{-1}$	10^{-3}
Viscosity of the fluid	η_f	$Pa.s$	10^{-3}
Electrokinetic coefficient	C_{ek}	$V.Pa^{-1}$	-2×10^{-5}
Pore space coefficient	m_p		6

117 countered when designing seismoelectric experiments. We show afterwards some results
118 based on experiments we performed during the last decade. In section 3, we come back
119 on the seismoelectric and seismomagnetic measurements we realized in a low noise labo-
120 ratory [*Bordes et al.*, 2006, 2008]. Eventually, in section 4, we evoke the results obtained
121 by *Bordes et al.* [2015] and *Holzhauer et al.* [2016] in order to quantitatively validate the
122 transfer function approach, for various fluid's conductivities and water saturations.

125 2 Designing seismoelectric experiments

126 The quantitative study of seismoelectric transfer functions needs carefully designed
127 experiments including simultaneous seismic and seismoelectric measurements. A well-
128 designed experiment is intended to be a downscaled analog of field surveys, and/or to
129 involve the same dissipation processes as in real conditions. When dealing with Pride's
130 theory, the key parameter will be the vicinity of the Biot frequency. For this purpose, a
131 compromise has to be sought by balancing frequency and petrophysical properties: the

nominal frequency has to be as close to/far from the Biot frequency as in field survey. In section 2.1, we show that the choice of sandbox experiments in the kiloHertz range is a comfortable compromise, by comparing the f/f_c ratio for various possible experiments. Quantitative measurements require the acquisition system to be carefully designed (section 2.2), seismic sensors to be well calibrated, the coupling with the porous sample to be the best as possible, and the electrodes and dipole length to be carefully chosen. Thus, we aim to check in section 2.3 the linearity of seismoelectric amplitude versus source energy. The choice of metallic electrodes, is discussed in section 2.4 and the reconstruction of dipoles using measurements referred to a common electrode (reference electrode) is discussed in section 2.5. Eventually we show the linearity of potential gradient to be unsatisfied for large dipoles and we make some suggestions on the best dipole length in section 2.6.

2.1 On the choice of sandbox experiments

When dealing with Pride's formulation, that is based on Biot's theory, the choice of the frequency range must be balanced against petrophysical properties involved in the Biot frequency f_c (see equation 9). Indeed, depending on the frequency f, relative fluid/solid motions may be controlled by viscous ($f/f_c < 1$) or inertial ($f/f_c > 1$) forces. The seismoelectric transfer functions are expected to reach their maximum magnitude in the viscous domain (low frequencies) and to drop at highest frequencies (see figure 1). In terms of seismoelectric transfer functions, field surveys at seismic frequencies might be ideal conditions provided that electrokinetic and signal-to-noise ratios are high enough.

Working at ultrasonic frequencies does not seem be the simplest way to experiment on seismoelectric phenomena. On the one hand because they stand in the inertial domain for which transfer functions are dropping, on the second hand because seismic waves are strongly damped due to combined scattering and attenuation. Nevertheless it is possible to work on such frequencies (higher than $20kHz$), for example in sandstone, by dealing with small samples [*Zhu et al.*, 2000]. In this case, the f/f_c ratio would stand around $10^1 - 10^2$ (see table 2) and the observations might be a nice analog of borehole measurements performed in the same frequency range.

Nevertheless, the f/f_c ratio for field studies at seismic frequencies stands around 10^{-3} (viscous domain) and upscaling the results from acoustic measurements to field sur-

Table 2. Comparison of key parameters in field and laboratory seismoelectric studies. Computation of the Biot frequency was performed for waterfilled sandstone and sand whose properties are given in table 1.

	Field surveys waterfilled sandstone	Ultrasonic waterfilled sandstone	Sandbox S_w=0.5	Sandbox S_w=1
Frequency				
$f\ (Hz)$	50	10^6	1000	1000
Biot's frequency				
$f_c\ (Hz)$	1.6×10^4	1.6×10^4	800	4000
$\mathbf{f/f_c}$	$\mathbf{3.14 \times 10^{-3}}$	**63**	**1.26**	$\mathbf{2.51 \times 10^{-1}}$

veys may be difficult. It is more recommended to use lower frequencies($1 - 10\ kHz$), *i.e.* closer to the Biot frequency. For this purpose, sandbox experiments have the advantage to use lower f/f_c values. Mechanical seismic sources may be driven by compressed air or weight drop, and are particularly well suited for emitting frequencies in the kiloHertz range. They generate higher energy than piezoelectric transducers with limited electromagnetic disturbances. Moreover, many shapes of sandbox experiments can be envisaged (depending on which propagation mode is required), and instrumentation is easy to install (seismic receivers, electrodes, saturation probes....) with satisfying mechanical coupling.

2.2 Solving impedance issues for electric measurements

When dealing with quantitative measurements of electrical potentials, the acquisition system must be carefully chosen and follow basic precautions. Indeed, its input impedance R_{in} must be very high compared to the impedance between the electrodes R_{dip}. The later can be easily measured for various length of dipoles: in the case the assumption $R_{dip} \ll R_{in}$ would be verified, the quantitative measurement of ΔV may be envisaged safely. In the opposite case, the equivalent resistance would be $R^{-1} = R_{dip}^{-1} + R_{in}^{-1}$ and the acquisition system would act as a tension divider. It would therefore be necessary to correct the measurement ΔV_m in order to obtain the real potential difference ΔV by:

$$\Delta V = \Delta V_m \frac{R_{dip} + R_{in}}{R_{in}} \tag{14}$$

Nevertheless, when dealing with various fluid conductivities and/or saturations, changes in R_{dip} may be very strong and the correction may become unrealistic. Thus, the best solution would be to increase the input impedance until 0.1 to 1 $G\Omega$ by custom-made preamplifiers that may also include gain or digital filtering [*Bordes et al.*, 2015] .

2.3 Checking the linearity of the coseismic effect for variable source magnitude

As shown in section 1, the conversion from seismic to electric energy follows a dynamic transfer function dropping with frequency (figure 1). A seismic source which waveform would be reproducible is therefore expected to be converted into a seismoelectric field which waveform should be reproducible as well. Eventually, changes in source's magnitude is expected to involve the same changes in seismoelectric amplitudes with a linear relation. This assumption is very important when stacking or normalizing processing are used, especially when dealing with mechanical sources that are less reproducible than piezoelectric sources. When designing the experiment *Bordes et al.* [2006, 2008], checked the maximum amplitudes recorded on a dipole for various source magnitudes, all other parameters being constant. As expected, the potential difference increases quasi-linearly with the source magnitude (figure 2). Thus, it makes sense normalizing seismic and seismoelectric records by the source magnitude. This normalization, that is possible only by systematically recording the source signal, allows a quantitative interpretation of amplitudes, even when changes in source magnitudes cannot be avoided.

2.4 Unpolarizable electrodes versus metallic electrodes

The question, whether or not non-polarising electrodes are needed in seismoelectric measurements, is often discussed. Metallic electrodes are generally not admitted for spontaneous potential surveys since they may be affected by biases due to polarisation effects. Indeed, these effects can be particularly strong at very low frequency when metallic electrodes are kept in a surrounding electrolyte for a very long time. Nevertheless, seismoelectrics consist in measuring transient potential gradients on very short times (typically few milliseconds) and polarisation issues cannot be addressed with the same point of view.

In field and laboratory seismoelectric studies, both electrode systems are used, assuming the polarisation effect to be poor. This issue has been addressed at field scale by

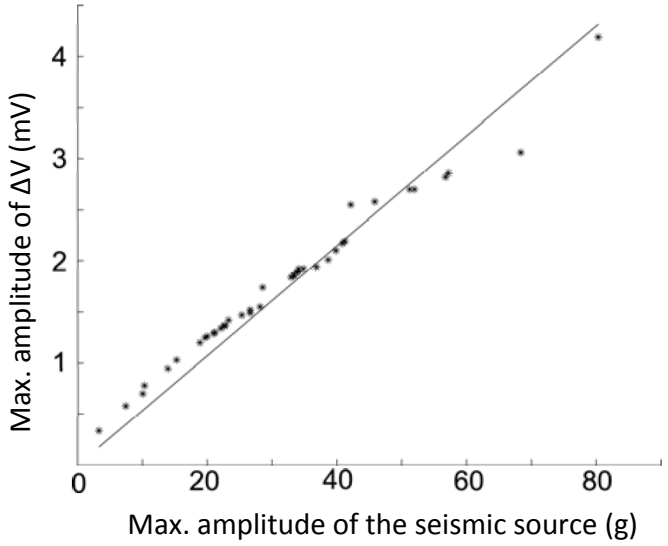

Figure 2. Checking the linearity of the coseismic effect in Fontainebleau sand for variable source magnitude (pneumatic device) [adapted from *Bordes*, 2005]

Beamish [1999] who used electrodes of three types: 1) stainless-steel (standard) electrodes, 2) lead rods, 3) non-polarizing Cu/CuSO4 electrodes. He concluded that the received voltages appear largely independent of electrode type as long as the ground contact resistance was no issue. Hence he would advocate for porous-pot electrodes only in arid environments, or advice to water the metal rods. Many other field studies used simple metallic electrodes on the surface or in boreholes [*Butler et al.*, 1996; *Mikhailov et al.*, 2000; *Garambois and Dietrich*, 2001; *Haines et al.*, 2007; *Strahser et al.*, 2007; *Dupuis and Butler*, 2006; *Dupuis et al.*, 2007]. Many laboratory studies were performed with metallic electrodes as well: [*Chen and Mu*, 2005; *Zhu et al.*, 1999, 2000; *Zhu and Toksöz*, 2005; *Dukhin et al.*, 2010; *Bordes et al.*, 2015]. Some authors used Ag/AgCl non-polarising electrodes in the laboratory [*Block and Harris*, 2006; *Bordes et al.*, 2006, 2008; *Schakel et al.*, 2011; *Smeulders et al.*, 2014] but did not discuss their absolute necessity, except *Zhu and Toksöz* [2013] who measured streaming potential and seismoelectric conversion on the same experiment.

Beamish's conclusions were confirmed by *Bordes* [2005] by comparing seismoelectric waveforms obtained by Ag/AgCl and silver electrodes. The datasets shown in figure 3 were obtained in two distinct experiments. The experimental apparatus was a vertical

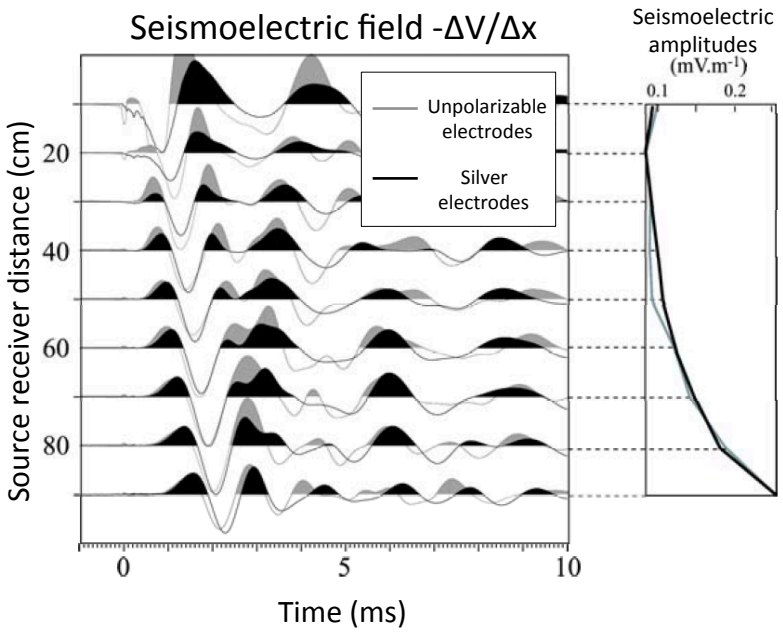

Figure 3. Comparison of seismoelectric signals obtained by unpolarizable and silver electrodes [adapted from *Bordes*, 2005]

column of quartz sand, filled of water from the lower extremity [*Bordes et al.*, 2006]. The main drawback of this apparatus is the fluid accumulation at the bottom of the column with a possible saturation gradient along the sample. This effect may be particularly strong in the upper part of the column. In the following, we therefore focus the comparison between both types of electrodes on offsets larger than $40cm$.

In this experiment, potential gradients were measured by referring to a common electrode located $95cm$ from the source, and the seismoelectric field was calculated as the ratio of potential gradient and dipole length ($E = -\Delta V/\Delta x$). All the signals shown in this figure were normalized by the trace maximum (for a clearer view of waveforms) and by the source amplitude (for correcting the source non-reproducibility). The maximum of the seismoelectric amplitudes is shown in the right part for a quantitative comparison. The saturation gradient along the column might explain the increase of seismoelectric amplitudes. Eventually the comparison of these datasets shows both signals to be very close in amplitude and waveform, the strong differences observed in later parts being probably due to a lack of reproducibility of the mechanical source. We conclude from this test both

non-polarising and metallic electrodes to be well suited for seismoelectric measurements, as initially suggested by *Beamish* [1999].

2.5 Local measurement versus dipole reconstruction

In field measurements, the seismoelectric acquisition consists of dipoles arrays, each dipole being composed of two electrodes located on either side of a seismic sensor. The dipole length l is chosen in order to provide the best signal to noise ratio, as large dipoles are tending to favour both seismoelectric signals and electrical ambiant noise. In this case, the local potential gradient measured by electrodes located at the offset x is:

$$\Delta V^{\mathrm{loc}}(x) = \left[V(x - \frac{l}{2}) - V(x + \frac{l}{2}) \right] \tag{15}$$

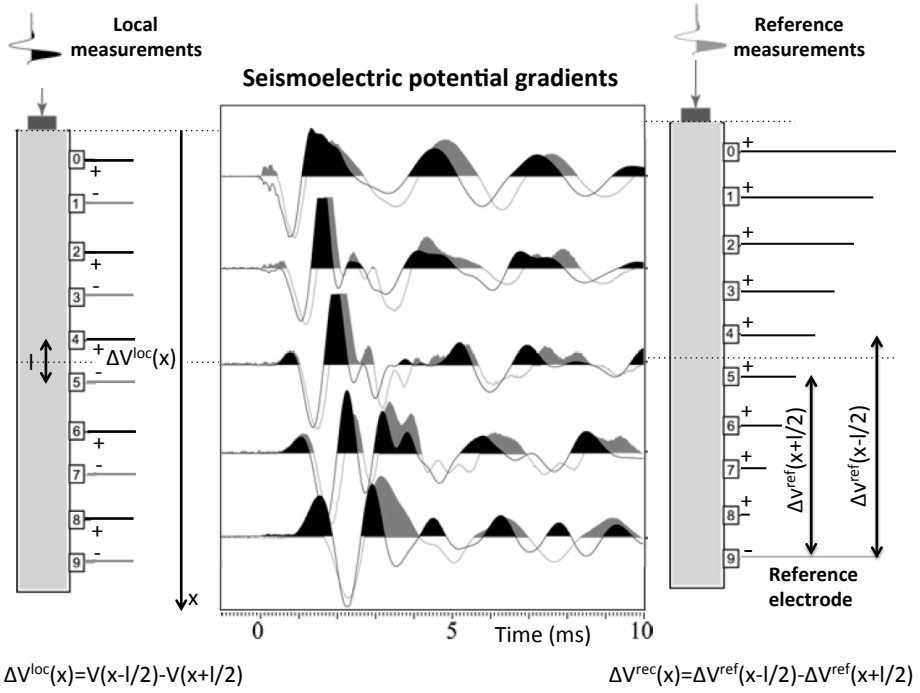

Figure 4. Comparison of local SE measurements with their reconstructed waform using a reference electrode [adapted from *Bordes*, 2005]

The main drawback of the local measurement is that datasets cannot be rearranged for testing other dipole geometries, since dipoles are completely independent from each others. A possible alternative is the measurement by referring to a common electrode. Hence, locating the electrodes every distance l, the potential gradient at offset x measured

by the reconstructed dipole of length l would be:

$$\Delta V^{\text{rec}}(x) = \left[V(x - \frac{l}{2}) - V(\text{ref})\right] - \left[V(x + \frac{l}{2}) - V(\text{ref})\right] \equiv \Delta V^{\text{loc}}(x). \tag{16}$$

Indeed, the reconstructed and local dipoles are expected to provide the same signal, which can be easily checked by operating both acquisitions, as shown in figure 4. This simple test shows both acquisition systems to be consistent, even if some discrepancies are observed in the later part of the signal. This test confirms the reference electrode system to be an interesting alternative to the local measurement.

From the initial reference measurement, it is afterwards possible to provide many datasets corresponding to other electrode configurations, for example with various dipole length (l, $2l$, $3l$...). Another disadvantage of the local dipoles is that many more electrodes have to be set up. It is therefore possible to process many more traces by using the reconstructed dipoles, for the same experimental setup, that is a very interesting point for understanding the various wavefronts travelling in the sample.

2.6 On the best electrode configuration

The effect of dipole geometry on the measurement of seismoelectric fields has been a pending issue ever since this phenomenon regained attention in the 90's. Various authors *Beamish* [1999]; *Strahser et al.* [2007] investigated, at a given point, the influence of the spacial distribution of electrodes on the estimate of electric field amplitudes. Indeed, estimating the local electric field by using its definition $\mathbf{E} = -\nabla V$ assumes the potential gradients to be measured between two points sufficiently close. In this case, isopotential curves are expected to be almost parallel between electrodes, *i.e.* the variations of potential are gradual and almost linear (null divergence). If this assumption is completed, the local amplitude of the electric field

$$E_x = -\Delta V / \Delta x \tag{17}$$

should not depend on the selected dipole-length, and the $\Delta V = f(l_{dip})$ curve should be linear ($\Delta x = l_{dip}$).

When dealing with seismoelectric fields, the shape of isopotential curves is completely driven by the original seismic wave and its characteristic wavelength λ. At a given time, signal reaching electrodes of dipoles larger than a quarter wavelength might be out of phase: the isopotential curves within the dipoles might be ungradual (bumps and holes)

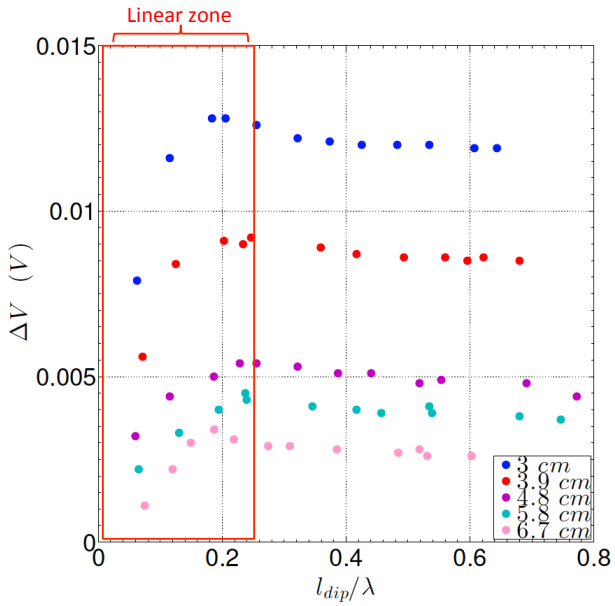

Figure 5. Checking the validity of seismoelectric field reconstruction from potential difference measurements [adapted from *Holzhauer et al.*, 2016]

and the $E_x = -\Delta V/\Delta x$ relation might be not adapted. This statement can be checked by using reconstructed dipoles of various lengths as proposed by *Holzhauer et al.* [2016]. In this experiment, seismoelectric potential gradients at various offsets were recorded by a dense electrodes array, allowing many different dipole-length l_{dip}. In figure 5, the maximum amplitudes of the first arrival ΔV are displayed as a function of l_{dip}/λ ratio and clearly show the linear relation to be obtained only for dipole smaller than a quarter wavelength (even a fifth for some traces). Eventually, *Holzhauer et al.* [2016] concluded that the smaller the dipole length is, the better the measurement of the electric field will be, as long as the signal to noise ratio remains sensible.

3 Measuring the seismomagnetic field

Whether seismoelectric measurements were performed in the laboratory or in the field, the measurement of the seismomagnetic field was rarely addressed [*Zhu and Toksöz*, 2005; *Bordes et al.*, 2006, 2008]. As shown in section 1, P waves are pure divergence and the corresponding seismoelectric field has no magnetic counterpart. The seismomagnetic field $\mathbf{B}$ is then expected to be coupled to the sole S waves, whose seismoelectric couplings

are very low (figure 1). Indeed, **B** is expected to be of very weak magnitude and the measurement seems possible only under very low electromagnetic magnetic noise.

The *Bordes et al.* [2006, 2008] experiments were therefore performed in a low noise underground laboratory (LSBB, Rustrel France) whose noise level was measured by *Gaffet et al.* [2003] to be lower than 2 $fT/\sqrt{Hz}$ above 10 Hz. The experimental apparatus was made of a porous sample, a seismic source, electric dipoles, two homemade fluxgate magnetometers and accelerometers located within the ultrashielded chamber. All electronic devices were located outside the chamber for avoiding electromagnetic disturbances from the instruments. Seismic and seismoelectric measurements were simultaneously performed in a common experiment whereas seismomagnetic field was recorded in a dedicated experiment. The experimental apparatus was carefully designed for avoiding any vibrations of sensors or metallic elements. Reproducibility was also ensured by using a controlled setup procedure, including sand packing and water filling.

These experiments eventually showed both seismoelectric and seismomagnetic field to be measurable in this very favorable environment (figure 6). Their electrokinetic origin was confirmed by checking that no coherent arrival was recorded in dry sand. In "fluid filled" sand, the first arrival of seismic and seismoelectric fields have the apparent velocity of a P wave [*Bordes et al.*, 2006] in a partially saturated compacted sand ($\simeq$ 1300 m/s). As for the seismomagnetic field, its apparent velocity is consistent with S waves propagating in the same medium ($\simeq$ 900 m/s). This experiment was an interesting step in the validation of Pride's theory since it confirms the existence of a measurable seismomagnetic field, most likely with an S wave apparent velocity. Nevertheless, measuring the 3 components of all fields would be a valuable improvement, since it would enable the evaluation of wave polarisation and would therefore confirm the identification of P and S waves.

4 Quantitative validation of Pride's transfer functions

4.1 Checking the effect of fluid's conductivity

Fluid conductivity is the most adjustable parameter in laboratory experiments: its change demands no great operation but to equilibrate the medium towards the wanted conductivity value by continuous water circulation. As early as the 70's, *Parkhomenko and Gaskarov* [1971] noted in their conclusions that "as the degree of mineralization of the solution saturating the rock increases, the magnitude of the E-effect is reduced approxi-

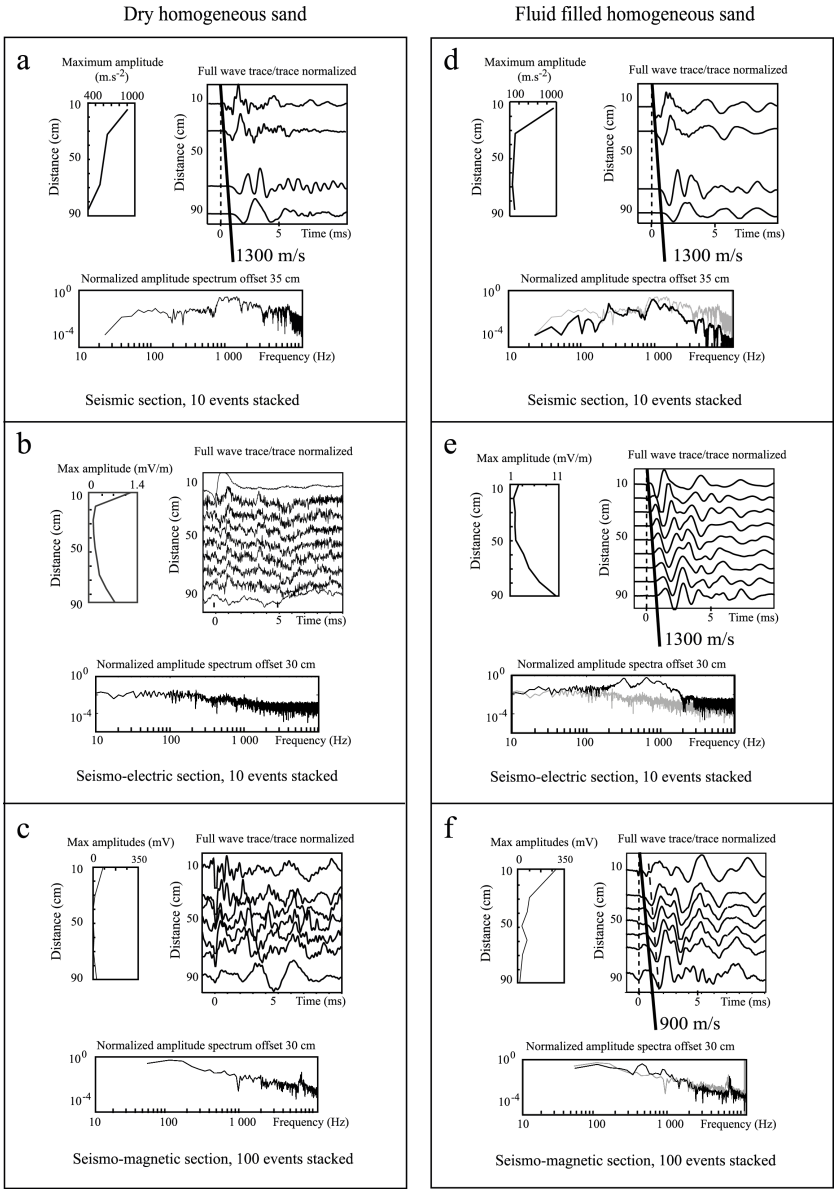

Figure 6. Seismic, seismoelectric and seismomagnetic signals recorded along a cylindrical sample in dry and fluid filled sand [adapted from *Bordes*, 2005]

mately exponentially". This effect was afterwards brought to light in the low-frequency approximation of the coseismic transfer function given by *Garambois and Dietrich* [2001]. Within the last decade, further similar studies have been conducted either on sand and glass beads [*Block and Harris*, 2006] or on Berea sandstone [*Zhu and Toksöz*, 2013] for frequencies reaching some tens of kilohertz.

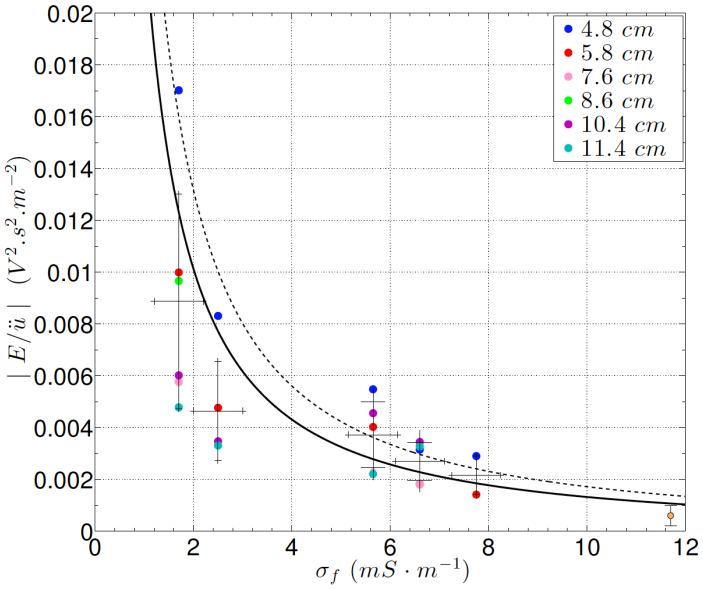

Figure 7. Seismoelectric transfer function as a function of fluid's conductivity measured in a sandbox experiment [adapted from *Holzhauer et al.*, 2016]. Theoretical curves at 0.5 kHz (dashed line) and 2 kHz (solid line) were obtained using the dynamic formulation of ψ_{Pf} including the *Jackson* [2010] model for saturation dependence of the electrokinetic coefficient.

Investigation of the transfer function dependence on fluid conductivity was also conducted by *Holzhauer et al.* [2016] for the quantitative validation of Pride's transfer functions (figure 7). In this experiment, the fluid conductivity was controlled by progressive addition of NaCl salts to eventually cover fluid conductivities ranging from 2.5 $mS \cdot m^{-1}$ to 10 $mS \cdot m^{-1}$. As σ_f increases, the seismoelectric amplitude drastically decreases (almost by one order of magnitude) when seismic amplitude remains mostly invariant, and the $|E/\ddot{u}|$ is therefore damping very fast. Eventually, experimental observations are consistent with theoretical predictions, both in order of magnitude and conductivity dependence of seismoelectric transfer functions.

4.2 Effect of water saturation in sands and dynamic compatibility phenomenon

Although the dependence of seismoelectromagnetic signals on fluid parameters (fluid's conductivity, pH, viscosity) were numerically and/or experimentally addressed, the impact of partial saturation has been rarely studied. However, full saturation is often not achieved in reservoirs, since they generally contain at least a few percents of gas or oil, strongly

influencing mechanical [*Bachrach and Nur*, 1998; *Bachrach et al.*, 1998; *Rubino and Holliger*, 2012] as well as electrical [*Archie et al.*, 1942] and electrokinetic [*Guichet et al.*, 2003; *Revil et al.*, 2007; *Jackson*, 2010; *Allegre et al.*, 2010; *Jougnot et al.*, 2012; *Allègre et al.*, 2012, 2015] properties of the medium. Field investigations were performed by *Strahser et al.* [2011] who measured both the seismoelectric coupling and the electrical impedance between electrodes and suggested that the water content should modify seismoelectromagnetic couplings. In the laboratory, *Parkhomenko et al.* [1964] measured the seismoelectric potential during water imbibition of dried rocks. Their results showed a dependence of the seismoelectric effect on water content, but they did not measure seismic displacements nor acceleration assuming that it should not vary with a reproducible seismic source. However it is admitted that seismic amplitudes should depend on water saturation due to specific dissipation phenomena *Carcione* [2007]; *Masson and Pride* [2007]; *Rubino and Holliger* [2012]. Indeed, the dependence of seismoelectric coupling should always be addressed in term of transfer function, accounting for seismic amplitudes variations, as discussed in section 1.

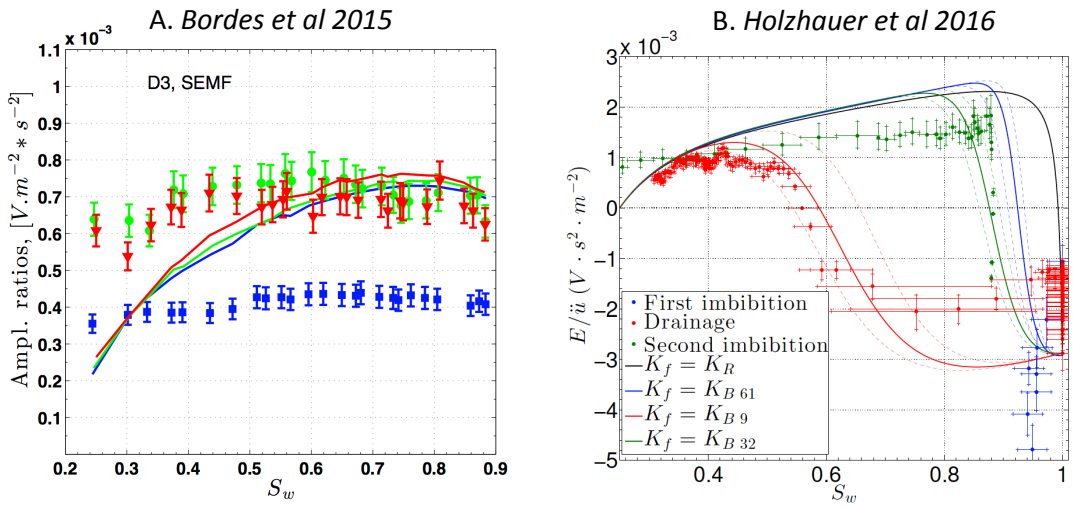

Figure 8. Theoretical and experimental seismoelectric transfer function as a function of fluid saturation for various offsets [A. adapted from *Bordes et al.*, 2015] and for different imbibition/drainage cycles [B. adapted from *Holzhauer et al.*, 2016]. In experiment A, theoretical curves are computed by using a systematic estimation of the dominant frequency (blue: offset=20cm, red: offset=30cm and green: offset=40cm). In experiment B, theoretical curves were obtained by a joint least-square inversion of velocities and seismoelectric transfer functions in order to estimate the best exponent in Brie's model. The best fit (bold lines) is surrounded by the curves obtained for a 10% misfit.

The effect of water saturation on seismoelectric transfer functions was studied in sandbox experiments by *Bordes et al.* [2015] and *Holzhauer et al.* [2016]. The goal was to compare laboratory data with theoretical predictions from *Pride* [1994] theory, extended to partial saturation by an effective fluid model as proposed in *Warden et al.* [2013]. The *Bordes et al.* [2015] experiment (A) focused on the $S_w = [0.3 - 0.9]$ range for various offsets, when *Holzhauer et al.* [2016] (experiment B) succeeded in reaching the full saturation (figure 8). These studies showed that the transfer functions behave as a plateau in the $S_w = [0.3 - 0.9]$ range as long as the fluid distribution remains homogeneous (all experiments from A and first imbibition from B). The seismoelectric transfer function at shortest offset was clearly lower than those measured at further ones in experiment A. This observation was not fully understood, but near-field effects were suspected. Eventually, the Pride theory extended to partial saturation succeeded in predicting the order of magnitude of the transfer functions.

By investigating the full saturation case, *Holzhauer et al.* [2016] obtained an original observation: the sign of the transfer function was changing at a specific saturation S^* related to the fluid distribution. This phenomenon can be recovered in theoretical transfer functions by accounting for fluid heterogeneities *via* Brie's formulation for the effective bulk modulus of the fluid [*Brie et al.*, 1995]. Hence, S^* is expected to be lower for an heterogeneous fluid (*i.e.* laid out in patches) than for an homogeneous onde (fine mixture of gas and water). Actually, the water was sucked out very rapidly during the drainage experiment and the formation of patches is very likely.

The S^* saturation corresponds to the peculiar state of "dynamic compatibility" predicted by *Biot* [1956a]. In his original paper, Biot evoked: "A remarkable property is the possible existence of a wave such that no relative motion occurs between fluid and solid". This condition is obtained when an equilibrium between elastic and dynamic constants is achieved. As suggested by *Hu et al.* [2009] this condition can be observed at a critical porosity, but it can be reached at a critical saturation as well. Eventually, under the dynamic compatibility condition, neither attenuation nor seismoelectric field may be observed since both solid and fluid are moving in-phase. The polarity change in seismoelectric transfer functions obtained by *Holzhauer et al.* [2016] is therefore an original observation of this poorly experienced phenomenon.

5 Conclusion

In the last decade, the potential of seismoelectrics for the geophysical characterization of porous media has been proven by the spectacular development of numerical, field and laboratory studies in litterature. The coseismic part of the seismoelectric field is often considered to be devoid of interest since it comes with the seismic field. Nevertheless, this phenomenon carries the signature of relative fluid motion within the pores that is involved in attenuation and dispersion of the seismic waves. A quantitative study of these seismoelectric fields may actually provide a powerful tool for experiencing various phenomena described by poroelastic theories. We would advise the transfer function approach as the best way to study the coseismic coupling since it neutralizes the effect of any changes in seismic amplitudes when monitoring any parameter variations.

This quantitative interpretation requires well designed experiments including calibrated seismic measurements and electric dipole which length and location must be carefully chosen. The choice of the frequency f must be balanced against the Biot frequency f_c in order to get a f/f_c ratio close to that of field studies. We showed the sandbox experiments in the kiloHertz range to be a reasonable analog of field studies at seismic frequencies. We would recommend to measure the potential difference by referring to a common reference electrode located as far as possible from the source: this method provides large datasets that can be rearranged for various dipole length. Metallic electrodes may be used, and the best dipole length seems to be smaller than a fifth wavelength for ensuring the fundamental relation $E = -\Delta V/\Delta x$ to be relevant.

In light of these recommendations, we performed a series of laboratory experiments in order to test some of Pride's expectations. For instance, by comparing seismomagnetic and seismoelectric fields in a sand column, we confirmed their respective coupling to S and fast P waves. We also showed the magnitude of theoretical transfer functions obtained from Pride's theory to be consistent with laboratory measurements, even under variable fluid conductivity and water saturation. We were also able to observe the "dynamic compatibility" predicted by Biot, this peculiar state in which both solid and fluid phases are moving in-phase.

All these experiments confirmed the coseismic part of seismoelectric fields to provide an interesting and powerful tool for investigating the effect of pore fluid on the seismic propagation in porous media. Many other studies might be considered. For exam-

ple, the study of patchy saturation might show a particular effect on seismoelectric phenomenon combining both coseismic and interface conversions at patches boundaries [*Jougnot et al.*, 2013]. Experiments focussing on very short offsets might also provide original observations of the diffusive part of the Biot slow wave [*Garambois and Dietrich*, 2013]. In future experiments, special efforts will have to be deployed for obtaining dynamical transfer functions, ideally on a large range of frequencies. Eventually, the recent development of various codes for the computation of the seismoelectric effect should provide great opportunities for improving the interpretation of both laboratory and field data.

Acknowledgments

This work was supported by the French Ministry of Higher Education and Research, the French National Research Agency (ANR Transek project), the Center for National Scientific Research (CNRS), the ISIFoR Institute, and the TOTAL company. We acknowledge technical staff involved in these studies: M. Auguste, D. Boyer, Y. Brun, A. Cavaillou, B. Guatarbes, J-M Martin, E. Normandin,V. Poydenot and P. Sénéchal.

References

Allegre, V., L. Jouniaux, F. Lehmann, and P. Sailhac (2010), Streaming potential dependence on water-content in fontainebleau sand, *Geophysical Journal International*, *182*(3), 1248–1266.

Allègre, V., F. Lehmann, P. Ackerer, L. Jouniaux, and P. Sailhac (2012), Modelling the streaming potential dependence on water content during drainage: 1. A 1D modelling of SP using finite element method, *Geophysical Journal International*, *189*, 285–295, doi:10.1111/j.1365-246X.2012.05371.x.

Allègre, V., L. Jouniaux, F. Lehmann, P. Sailhac, and R. Toussaint (2015), Influence of water pressure dynamics and fluid flow on the streaming-potential response for unsaturated conditions, *Geophysical Prospecting*, *63*, 694–712, doi:10.1111/1365-2478.12206.

Archie, G. E., et al. (1942), The electrical resistivity log as an aid in determining some reservoir characteristics, *Transactions of the AIME*, *146*(01), 54–62.

Bachrach, R., and A. Nur (1998), High-resolution shallow-seismic experiments in sand, part i: Water table, fluid flow, and saturation, *Geophysics*, *63*(4), 1225–1233.

Bachrach, R., J. Dvorkin, and A. Nur (1998), High-resolution shallow-seismic experiments in sand, part ii: Velocities in shallow unconsolidated sand, *Geophysics*, *63*(4), 1234–

1240.

Barriere, J., C. Bordes, D. Brito, P. Sénéchal, and H. Perroud (2012), Laboratory monitoring of p waves in partially saturated sand, *Geophysical Journal International*, *191*(3), 1152–1170.

Beamish, D. (1999), Characteristics of near-surface electrokinetic coupling, *Geophysical Journal International*, *137*(1), 231–242.

Biot, M. A. (1956a), Theory of propagation of elastic waves in a fluid-saturated porous solid. i. low-frequency range, *The Journal of the acoustical Society of america*, *28*(2), 168–178.

Biot, M. A. (1956b), Theory of propagation of elastic waves in a fluid-saturated porous solid. ii. higher frequency range, *the Journal of the Acoustical Society of America*, *28*(2), 179–191.

Block, G. I., and J. G. Harris (2006), Conductivity dependence of seismoelectric wave phenomena in fluid-saturated sediments, *Journal of Geophysical Research: Solid Earth*, *111*(B1).

Bolève, A., A. Revil, F. Janod, J. Mattiuzzo, and A. Jardani (2007), A new formulation to compute self-potential signals associated with ground water flow, *Hydrology and Earth System Sciences Discussions*, *4*(3), 1429–1463.

Bordes, C. (2005), Etude expérimentale des phénomènes transitoires sismo-électromagnétiques: Mise en oeuvre au laboratoire souterrain de rustrel, pays d'apt, Ph.D. thesis, Université Joseph-Fourier-Grenoble I.

Bordes, C., L. Jouniaux, M. Dietrich, J.-P. Pozzi, and S. Garambois (2006), First laboratory measurements of seismo-magnetic conversions in fluid-filled fontainebleau sand, *Geophysical Research Letters*, *33*(1).

Bordes, C., L. Jouniaux, S. Garambois, M. Dietrich, J.-P. Pozzi, and S. Gaffet (2008), Evidence of the theoretically predicted seismo-magnetic conversion, *Geophysical Journal International*, *174*(2), 489–504.

Bordes, C., P. Sénéchal, J. Barrière, D. Brito, E. Normandin, and D. Jougnot (2015), Impact of water saturation on seismoelectric transfer functions: a laboratory study of coseismic phenomenon, *Geophysical Journal International*, *200*(3), 1317–1335.

Brie, A., F. Pampuri, A. Marsala, O. Meazza, et al. (1995), Shear sonic interpretation in gas-bearing sands, in *SPE Annual Technical Conference and Exhibition*, Society of Petroleum Engineers.

Butler, K. E., R. D. Russell, A. W. Kepic, and M. Maxwell (1996), Measurement of the seismoelectric response from a shallow boundary, *Geophysics*, *61*(6), 1769–1778.

Carcione, J. M. (2007), *Wave fields in real media: Wave propagation in anisotropic, anelastic, porous and electromagnetic media*, vol. 38, Elsevier.

Chen, B., and Y. Mu (2005), Experimental studies of seismoelectric effects in fluid-saturated porous media, *Journal of Geophysics and Engineering*, *2*(3), 222.

Dukhin, A. S., P. J. Goetz, and M. Thommes (2010), Seismoelectric effect: A non-isochoric streaming current. 1. experiment, *Journal of colloid and interface science*, *345*(2), 547–553.

Dupuis, J., and K. Butler (2006), Vertical seismoelectric profiling in a borehole penetrating glaciofluvial sediments, *Geophysical Research Letters*, *33*(16).

Dupuis, J. C., K. E. Butler, and A. W. Kepic (2007), Seismoelectric imaging of the vadose zone of a sand aquifer, *Geophysics*, *72*(6), A81–A85.

Frenkel, J. (2005), On the theory of seismic and seismoelectric phenomena in a moist soil, *Journal of Engineering Mechanics*, *131*(9), 879–887.

Gaffet, S., Y. Guglielmi, J. Virieux, G. Waysand, A. Chwala, R. Stolz, C. Emblanch, M. Auguste, D. Boyer, and A. Cavaillou (2003), Simultaneous seismic and magnetic measurements in the low-noise underground laboratory (lsbb) of rustrel, france, during the 2001 january 26 indian earthquake, *Geophysical Journal International*, *155*(3), 981–990.

Garambois, S., and M. Dietrich (2001), Seismoelectric wave conversions in porous media: Field measurements and transfer function analysis, *Geophysics*, *66*(5), 1417–1430.

Garambois, S., and M. Dietrich (2002), Full waveform numerical simulations of seismoelectromagnetic wave conversions in fluid-saturated stratified porous media, *Journal of Geophysical Research: Solid Earth*, *107*(B7).

Garambois, S., and M. Dietrich (2013), Observation of the diffuse biot slow wave via its electrokinetic coupling: a numerical perspective, in *Poromechanics V: Proceedings of the Fifth Biot Conference on Poromechanics*, pp. 282–291, ASCE.

Guan, W., and H. Hu (2008), Finite-difference modeling of the electroseismic logging in a fluid-saturated porous formation, *Journal of computational physics*, *227*(11), 5633–5648.

Guichet, X., L. Jouniaux, and J.-P. Pozzi (2003), Streaming potential of a sand column in partial saturation conditions, *Journal of Geophysical Research: Solid Earth*, *108*(B3).

Haines, S. S., S. R. Pride, S. L. Klemperer, and B. Biondi (2007), Seismoelectric imaging of shallow targets, *Geophysics*, *72*(2), G9–G20.

Holzhauer, J., D. Brito, C. Bordes, Y. Brun, and B. Guatarbes (2016), Experimental quantification of the seismoelectric transfer function and its dependence on conductivity and saturation in loose sand, *Geophysical Prospecting*, pp. n/a–n/a, doi:10.1111/1365-2478.12448.

Hu, H., K. Wang, and J. Wang (2000), Simulation of an acoustically induced electromagnetic field in a borehole embedded in a porous formation, *Tech. rep.*, Massachusetts Institute of Technology. Earth Resources Laboratory.

Hu, H., Y. Gao, et al. (2009), The electric field induced by the fast p-wave and its nonexistence in a dynamically compatible porous medium, in *2009 SEG Annual Meeting*, Society of Exploration Geophysicists.

Jackson, M. D. (2010), Multiphase electrokinetic coupling: Insights into the impact of fluid and charge distribution at the pore scale from a bundle of capillary tubes model, *Journal of Geophysical Research: Solid Earth*, *115*(B7).

Johnson, D. L., J. Koplik, and R. Dashen (1987), Theory of dynamic permeability and tortuosity in fluid-saturated porous media, *Journal of fluid mechanics*, *176*, 379–402.

Jougnot, D., N. Linde, A. Revil, and C. Doussan (2012), Derivation of soil-specific streaming potential electrical parameters from hydrodynamic characteristics of partially saturated soils, *Vadose Zone Journal*, *11*(1), 0–0.

Jougnot, D., J. Rubino, M. R. Carbajal, N. Linde, and K. Holliger (2013), Seismoelectric effects due to mesoscopic heterogeneities, *Geophysical Research Letters*, *40*(10), 2033–2037.

Jouniaux, L., and T. Ishido (2012), Electrokinetics in earth sciences: a tutorial, *International Journal of Geophysics*, *2012*.

Jouniaux, L., and F. Zyserman (2015), Reply to comment by a. revil on" seismo-electrics, electro-seismics, and seismo-magnetics for earth sciences" by l. jouniaux and f. zyserman, *Solid Earth Discussions*, *7*, C1274–C1274.

Jouniaux, L., and F. Zyserman (2016), A review on electrokinetically induced seismoelectrics, electro-seismics, and seismo-magnetics for earth sciences, *Solid Earth*, *7*(1), 249.

Masson, Y. J., and S. R. Pride (2007), Poroelastic finite difference modeling of seismic attenuation and dispersion due to mesoscopic-scale heterogeneity, *Journal of Geophysical*

Research: Solid Earth, *112*(B3).

Mikhailov, O. V., J. Queen, and M. N. Toksöz (2000), Using borehole electroseismic measurements to detect and characterize fractured (permeable) zones, *Geophysics*, *65*(4), 1098–1112.

Müller, T. M., and B. Gurevich (2004), One-dimensional random patchy saturation model for velocity and attenuation in porous rocks, *Geophysics*, *69*(5), 1166–1172.

Müller, T. M., B. Gurevich, and M. Lebedev (2010), Seismic wave attenuation and dispersion resulting from wave-induced flow in porous rocks?a review, *Geophysics*, *75*(5), 75A147–75A164.

Overbeek, J. T. G. (1952), Electrochemistry of the double layer, *Colloid science*, *1*, 115–193.

Parkhomenko, E., and I. Gaskarov (1971), Borehole and laboratory studies of the seismoelectric effect of the second kind in rocks, *Izvestiya, Earth Physics*, *9*, 663–666.

Parkhomenko, I., C. Tsze-San, and C. CHIEN-SAN (1964), A study of the influence of moisture on the magnitude of the seismoelectric effect in sedimentary rocks by a laboratory method, *Bull.(Izv.) Acad. Sci., USSR, Geophys. Ser*, *2*, 115–118.

Pride, S. (1994), Governing equations for the coupled electromagnetics and acoustics of porous media, *Physical Review B*, *50*(21), 15,678.

Pride, S. R., and J. G. Berryman (2003a), Linear dynamics of double-porosity dual-permeability materials. i. governing equations and acoustic attenuation, *Physical Review E*, *68*(3), 036,603.

Pride, S. R., and J. G. Berryman (2003b), Linear dynamics of double-porosity dual-permeability materials. ii. fluid transport equations, *Physical Review E*, *68*(3), 036,604.

Pride, S. R., and M. W. Haartsen (1996), Electroseismic wave properties, *The Journal of the Acoustical Society of America*, *100*(3), 1301–1315.

Revil, A., and A. Jardani (2010), Seismoelectric response of heavy oil reservoirs: theory and numerical modelling, *Geophysical Journal International*, *180*(2), 781–797.

Revil, A., and H. Mahardika (2013), Coupled hydromechanical and electromagnetic disturbances in unsaturated porous materials, *Water resources research*, *49*(2), 744–766.

Revil, A., N. Linde, A. Cerepi, D. Jougnot, S. Matthäi, and S. Finsterle (2007), Electrokinetic coupling in unsaturated porous media, *Journal of Colloid and Interface Science*, *313*(1), 315–327.

Revil, A., G. Barnier, M. Karaoulis, P. Sava, A. Jardani, and B. Kulessa (2013), Seismoelectric coupling in unsaturated porous media: theory, petrophysics, and saturation front localization using an electroacoustic approach, *Geophysical Journal International*, *196*(2), 867–884.

Rubino, J. G., and K. Holliger (2012), Seismic attenuation and velocity dispersion in heterogeneous partially saturated porous rocks, *Geophysical Journal International*, *188*(3), 1088–1102.

Santos, J. E., F. I. Zyserman, and P. M. Gauzellino (2012), Numerical electroseismic modeling: a finite element approach, *Applied Mathematics and Computation*, *218*(11), 6351–6374.

Schakel, M., D. Smeulders, E. Slob, and H. Heller (2011), Laboratory measurements and theoretical modeling of seismoelectric interface response and coseismic wave fields, *Journal of Applied Physics*, *109*(7), 074,903.

Smeulders, D., N. Grobbe, H. Heller, and M. Schakel (2014), Seismoelectric conversion for the detection of porous medium interfaces between wetting and nonwetting fluids, *Vadose Zone Journal*, *13*(5).

Strahser, M., L. Jouniaux, P. Sailhac, P.-D. Matthey, and M. Zillmer (2011), Dependence of seismoelectric amplitudes on water content, *Geophysical Journal International*, *187*(3), 1378–1392.

Strahser, M. H., W. Rabbel, and F. Schildknecht (2007), Polarisation and slowness of seismoelectric signals: a case study, *Near Surface Geophysics*, *5*(2), 97–114.

Warden, S., S. Garambois, P. Sailhac, L. Jouniaux, and M. Bano (2012), Curvelet-based seismoelectric data processing, *Geophysical Journal International*, *190*(3), 1533–1550.

Warden, S., S. Garambois, L. Jouniaux, D. Brito, P. Sailhac, and C. Bordes (2013), Seismoelectric wave propagation numerical modelling in partially saturated materials, *Geophysical Journal International*, *194*(3), 1498–1513.

Zhu, Z., and M. N. Toksöz (2005), Seismoelectric and seismomagnetic measurements in fractured borehole models, *Geophysics*, *70*(4), F45–F51.

Zhu, Z., and N. Toksöz (2013), Experimental measurements of the streaming potential and seismoelectric conversion in berea sandstone, *Geophysical Prospecting*, *61*(3), 688–700.

Zhu, Z., M. W. Haartsen, and M. N. Toksöz (1999), Experimental studies of electrokinetic conversions in fluid-saturated borehole models, *Geophysics*, *64*(5), 1349–1356.

Zhu, Z., M. W. Haartsen, and M. Toksöz (2000), Experimental studies of seismoelectric conversions in fluid-saturated porous media, *Journal of Geophysical Research: Solid Earth*, *105*(B12), 28,055–28,064.

Zyserman, F., L. Jouniaux, S. Warden, and S. Garambois (2015), Borehole seismoelectric logging using a shear-wave source:Possible application to CO_2 disposal?, *International Journal of Greenhouse Gas Control*, *33*, 82–102, doi:10.1016/j.ijggc.2014.12.009.

Zyserman, F. I., P. M. Gauzellino, and J. E. Santos (2010), Finite element modeling of shte and psvtm electroseismics, *Journal of applied geophysics*, *72*(2), 79–91.

Zyserman, F. I., P. M. Gauzellino, and J. E. Santos (2012), Numerical evidence of gas hydrate detection by means of electroseismics, *Journal of Applied Geophysics*, *86*, 98–108.